Materials Chemistry and Physics 149-150 (2015) 34–42

Contents lists available at ScienceDirect

Materials Chemistry and Physics

journal homepage: www.elsevier.com/locate/matchemphys

Synthesis and fabrication of Y_2O_3:Tb^{3+} and Y_2O_3:Eu^{3+} thin films for electroluminescent applications: Optical and structural characteristics

G. Alarcón-Flores [a, *], M. García-Hipólito [b], M. Aguilar-Frutis [a], S. Carmona-Téllez [c], R. Martinez-Martinez [e], M.P. Campos-Arias [a], E. Zaleta-Alejandre [f], C. Falcony [d]

[a] Centro de Investigación en Ciencia Aplicada y Tecnología Avanzada, IPN, Legaría 694, Irrigación, C.P. 11500, México D.F., Mexico
[b] Instituto de Investigaciones en Materiales, UNAM, Apdo. Postal 70-360, Delegación Coyoacán, C.P. 04150, México D.F., Mexico
[c] Instituto de Física, UNAM, Coyoacán, C.P. 04150, México D.F., Mexico
[d] Departamento de Física, CINVESTAV, Apdo. Postal 14-470, Delegación Gustavo A. Madero, C.P. 07000, México D.F., Mexico
[e] Universidad Tecnológica de la Mixteca, Carretera Acatlima Km 2.5, Huajuapan de León Oaxaca, C.P. 69000, México, Mexico
[f] Universidad Autónoma del Estado de Hidalgo-Escuela Superior de Apan, Carretera Apan-Calpulalpan Km. 8, C.P. 43920, Apan, Hidalgo, Mexico

HIGHLIGHTS

- Terbium, europium and yttrium β diketonates have been synthesized.
- Luminescent thin films of Y_2O_3:Tb^{3+} and Y_2O_3:Eu^{3+} were obtained.
- Optical and structural characteristics of these thin films are presented.
- The films had a refractive index (1.81) and low average surface roughness (~62 Å).

ARTICLE INFO

Article history:
Received 28 March 2014
Received in revised form
29 July 2014
Accepted 22 September 2014
Available online 8 October 2014

Keywords:
Polycrystalline films
Spray pyrolysis
Photoluminescence
Cathodoluminescence

ABSTRACT

Terbium, europium and yttrium β diketonates have been synthesized from acetylacetone and inorganic metal salts and used as precursors for the deposition of Tb^{3+} or Eu^{3+} doped Y_2O_3 polycrystalline films by the ultrasonic spray pyrolysis technique. The films were deposited on c-Si substrates at temperatures in the 400–550 °C range. The optical and structural characterization of these films as a function of substrate temperature and Tb^{3+} and Eu^{3+} concentration was carried out by means of photoluminescence (PL), cathodoluminescence (CL), infrared (IR), ellipsometry, and UV–visible spectroscopy and atomic force microscopy (AFM), energy dispersive spectroscopy (EDS) and X ray diffraction (XRD) measurements respectively. The PL intensity from these films was found to depend on deposition temperature. Films deposited above 450 °C exhibited the characteristic PL peaks associated with either Tb^{3+} or Eu^{3+} intra electronic energy levels transitions. The most intense PL emission was found for dopant concentration of 10 at% for Tb^{3+} and at 8 at% for Eu^{3+} ions into precursor solution. In both cases concentration quenching of the PL emission was observed for concentrations above these values. The films had a refractive index (1.81), low average surface roughness (~62 Å) and a UV–Vis. transmission of the order of 90 %T.

1. Introduction

Metalorganic complexes such as metal β diketonates also called acetylacetonates are of great interest as precursors on chemically based deposition processes because of their excellent chemical and physical properties such as their high volatility and low decomposition temperature. The β diketonates have been used for metallic particle synthesis [1], as well as metalorganic vapor sources for deposition of metal oxide thin films [2,3]. The use of metalorganic precursors results in most film deposition methods in low surface roughness, better adhesion to the substrate, dense and relatively clean films, with better thermal stability and higher lateral resolution [4]. One of these methods is the ultrasonic spray pyrolysis (USP) technique that compared to others, chemical vapor deposition, sputtering deposition, pulsed laser deposition, for instance [5], has advantages like relatively low cost and industrial

* Corresponding author.
E-mail address: alar_fbeto@yahoo.com (G. Alarcón-Flores).

http://dx.doi.org/10.1016/j.matchemphys.2014.09.020
0254-0584/

scalability to large-area deposition of these films. On the other hand, wide band-gap metal oxides such as: Al_2O_3 (gap = 5.8 eV) [6], HfO_2 (gap = 5.4 eV) [7], Y_2O_3 (gap = 5.5 eV) [8] are often used as host lattice to incorporate optical activator ions, because of their high chemical and thermal stability, high resistance to cathode rays, among others. Yttria (Y_2O_3), in particular, is a cubic crystalline material with high melting temperature (2410 °C), large UV–Vis-IR transmittance (from 280 nm to 8 μm [9]), wide bandgap (5.5 eV) and high crystalline stability [8]. It has been used as host lattice for the manufacture of scintillators, lasers, optical fiber used in communications as well as nanocrystalline phosphors (luminescent properties of nanocrystalline phosphors might be quite different from their bulk counterpart and so their properties can be improved to expand their applications). Due to its high dielectric constant, yttria may be used in devices for flat panel displays applications (FED and PD), using electric fields much lower than those applied in the normal display devices [10]. Nanocrystalline phosphors generally have a higher efficiency which can be achieved with low voltages; therefore, they are ideal candidates for flat display devices [11]. In addition, application such as high definition televisions (HDTV) requires phosphors with small particle size, distribution size uniformity and high light intensity output without saturation [10]. Yttria films are in general, relevant for applications in field emission displays (FEDs) [12], Eu^{3+} doped Y_2O_3 is a red phosphor mainly used for FEDs. In this work the synthesis of β diketonates and their use as precursors to obtain Y_2O_3:Tb^{3+} and Y_2O_3:Eu^{3+} films by the USP method, is described. Additionally, the optical and structural characteristics of these resulting films as a function of deposition substrate temperature, and Tb^{3+} and Eu^{3+} concentration are presented as well.

2. Experimental

2.1. Synthesis of yttrium β diketonate [Y(acac)$_3$]

A solution of 3.83 g of $Y(NO)_3$ in 15 ml of bi-distilled water and 10 ml of methanol was placed in an ice bath, and then 3 ml of acetylacetone and 3 ml of propylene oxide were added. The pH was increased to 7 by adding, drop wise, concentrated NH_4OH, stirring for 45 min, until a light yellow precipitate was formed and then it was vacuum filtered. The powder obtained was then dried at 80 °C for four hours as described by W. Sheng-Yue, and T. E. Banach [13,14]. The synthetized compound was identified as yttrium β diketonate by means of proton nuclear magnetic resonance ^{1}H NMR (Bruker-Avance System 300 MHz instrument), Mass Spectrometry MS (Jeol AX505HA spectrophotometer), infrared spectroscopy IR (Perkin Elmer spectrum one). Its spectroscopic data and structural formula are:

^{1}H NMR (p.p.m): 1.74 (6H, s), 5.21 (1H, s).

MS (m/z): M^+ 386 (44.6%), 371 (3.1%) (M^+–15), 287 (100%) (M^+–99).

IR νmax (cm^{-1}) 1570 ν (C=O) and ν (C=C), 525 ν (C=C) and ν (C=O), 535 (MO).

2.2. Synthesis of terbium and europium β diketonates [Tb(acac)$_3$ and Eu(acac)$_3$]

Synthesis of terbium and europium β diketonates was carried out using terbium and europium chloride as raw precursor materials, respectively, following a similar procedure as the one used in the synthesis of yttrium β diketonate, described above. Spectroscopic data of IR and ^{1}H NMR of terbium and Europium β diketonate are similar to the yttrium β diketonate. However the MS were different because of the terbium and europium β diketonates molecular ion (M^+) are equal to 456 and 449 respectively. The molecular fragmentations are similar to yttrium β diketonate [4].

2.3. Synthesis of Y_2O_3:Tb^{3+} and Y_2O_3:Eu^{3+} thin films

To obtain Ln^{3+} doped films, yttrium β diketonate terbium and europium β diketonates, synthetized as described above, were used as precursors dissolved in N, N-dimethylformamide (DMF) [C_3H_7ON, JT Baker and purity of 99.96%]. For Y_2O_3:Tb^{3+} thin films, a 0.03 M solution of Y(acac)$_3$ was prepared (dissolving 1.16 g in 100 ml of DMF) and Tb(acac)$_3$ was added at different atomic percentages: 0, 2, 5, 10 and 15 at%. In the case of Y_2O_3:Eu^{3+} films, a solution 0.06 M of Y(acac)$_3$ was prepared by dissolving 2.32 g in 100 ml of DMF and Eu(acac)$_3$ was added at different atomic percentages: 0, 2, 5, 8, 10 and 12 at%. The films were deposited using the ultrasonic spray pyrolysis technique on crystalline silicon substrates of 1.5 × 1.5 cm at temperatures in the 400–550 °C range, for 15 min.

2.4. Optical and structural characterization

PL spectra were obtained with a SPEX Fluoro-Max-P spectrofluorimeter. CL measurements were performed in a stainless steel vacuum chamber with a cold cathode electron gun (Luminoscope, model ELM-2 MCA, RELION Co.). The diameter of the electron beam spot on the film was approximately 3 mm. The emitted light was collected by an optical fiber and fed into the SPEX Fluoro-Max-P spectrofluorimeter. The applied current of electron beam was 0.05 mA with an accelerating voltage in the range of 3–10 kV. All the luminescence measurements were performed at room temperature. Index of refraction and thickness of the deposited films were measured by ellipsometry (Gaertner LSE stokes ellipsometer), at 632 nm. A Siemens D-5000 X-ray diffraction system with CuK_α radiation (λ = 1.5406 Å) was used for the determination of the crystalline structure. Nanocrystalline sizes of films were estimated using the equation (1) (Scherrer's formula) [15].

$$T = \frac{0.9\lambda}{BCos\theta_B} \tag{1}$$

Where:

T = Crystallite size.
λ = Wavelength of CuK_α radiation.
B = Corrected half width of the diffraction peak.
θ_B = The Bragg's angle in radians.

Optical transmission spectra were obtained from films deposited on quartz substrates. An UV–vis spectrophotometer (Cary 50) in the 200–900 nm range was used for this purpose. Surface morphology of the films was determined by Atomic Force Microscope (Veeco CP research). The average roughness as well as the statistical analysis of the images is performed with the AFM Software. The average roughness is calculated using the following expression (Eq. (2)) over the analyzed area.

$$R_{ave} = \sum_{n=1}^{N} \frac{|z_n - \bar{z}|}{N} \tag{2}$$

Where:

R_{ave} = Average roughness.
$\bar{z}$ = mean z height.

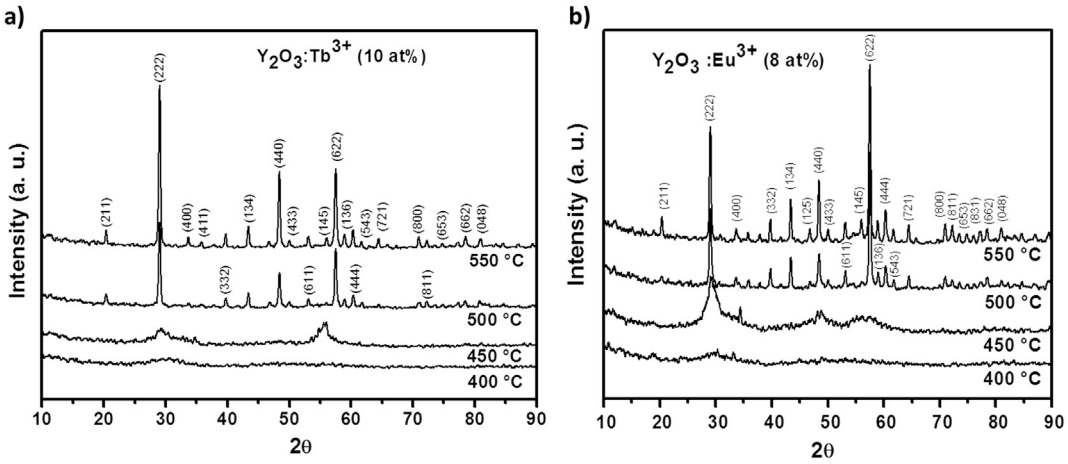

Fig. 1. X-ray diffractograms for 1a) Y_2O_3:Tb^{3+} and 1b) Y_2O_3:Eu^{3+} thin films deposited at temperatures from 400 to 550 °C.

3. Results and discussion

X-ray diffraction patterns for the deposited films are plotted in Fig. 1 for the different deposition temperatures and for.

a) Y_2O_3:Tb^{3+} and b) Y_2O_3:Eu^{3+} films. In both cases, at low temperatures 400 and 450 °C the films are amorphous and at temperatures of 500 and 550 °C the films become polycrystalline with a the Y_2O_3 cubic phase (JCPDS card number 43-1036). For both thin films the diffraction peaks are at 2θ: 29.04, 43.29, 48.39, and 57.54 which correspond to the planes (222), (134), (440) and (622) respectively. The Y_2O_3:Tb^{3+} samples present a (222) preferential orientation while the Y_2O_3:Eu^{3+} present a (622) preferential orientation, these peaks were used for the estimation the crystalline grain size using Scherrer's formula. The average grain size values were 23 and 24 nm for Y_2O_3:Tb^{3+} films and 22 and 26 nm for Y_2O_3:Eu^{3+} films deposited at 500 and 550 °C, respectively.

The IR spectra for Y_2O_3:Tb^{3+} and Y_2O_3:Eu^{3+} films synthesized in the 400–550 °C range are shown in Fig. 2 a and 2b respectively. They show two overlapped bands which are located approximately at 1405 and 1525 cm^{-1}; assigned to δ (CH_3) and ν (C=O) coupled with ν (C=C) vibrations, respectively [16,17]. The band at 872 cm^{-1} can be assigned to π (CH). These three bands are characteristic of the terbium, europium and yttrium β diketonates indicating an incomplete decomposition of the precursors during the films deposition process, especially at low temperatures [4]. Also, is important to note that these bands decrease significantly with increasing temperature, indicating that there is a large elimination of organic remains. The presence of organic residues, have already been reported in the films deposited using organic precursors and spray pyrolysis [18,19] and sol–gel [20] deposition techniques. A broad band around 345 cm^{-1} is also observed at low deposition temperatures, this band is increased and it splits, when the temperature is increased, in three well defined peaks located at about 300, 336, 372 cm^{-1}, also another peak is observed at about 557 cm^{-1}. All these peaks are assigned to Y–O stretching vibration indicating that the Y_2O_3 host lattice has been formed [21,22]. The improvement of the intensity of the Y–O bonds related peaks at high temperatures (500 and 550 °C) is in agreement with the improvement of the crystalline structure of the films shown in the X-ray results for these temperatures. The IR spectra also show two bands located approximately at 2848 and 2921 cm^{-1}. These bands can be assigned to stretching vibration mode of methyl group CH_3 (ν) [17]. Finally, it also is observed a weak band centered 3500 cm^{-1} corresponding to the O–H bonding, most likely duo to H_2O molecules adsorbed on film surface [4,20].

Fig. 3a and b show the atomic force microscopy images for Y_2O_3:Tb^{3+} and Y_2O_3:Eu^{3+} films, respectively. The images show a 4μ × 4μ surface area for films deposited in the 400–550 °C temperature range. All films in general show granular morphology with a very low average surface roughness in the 9.49 to 76.2 Å range for

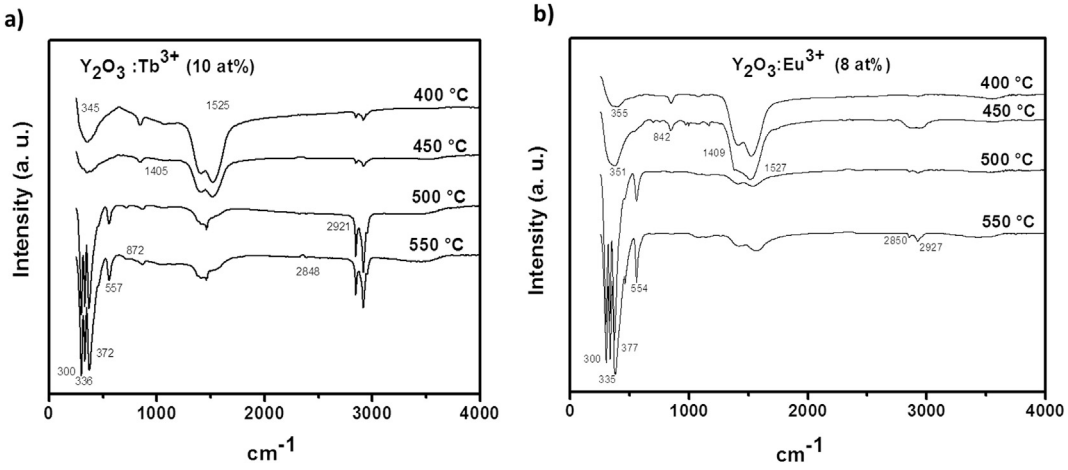

Fig. 2. Infrared spectra for 2a) Y_2O_3:Tb^{3+} and 2b) Y_2O_3:Eu^{3+} thin films deposited at temperatures from 400 to 550 °C.

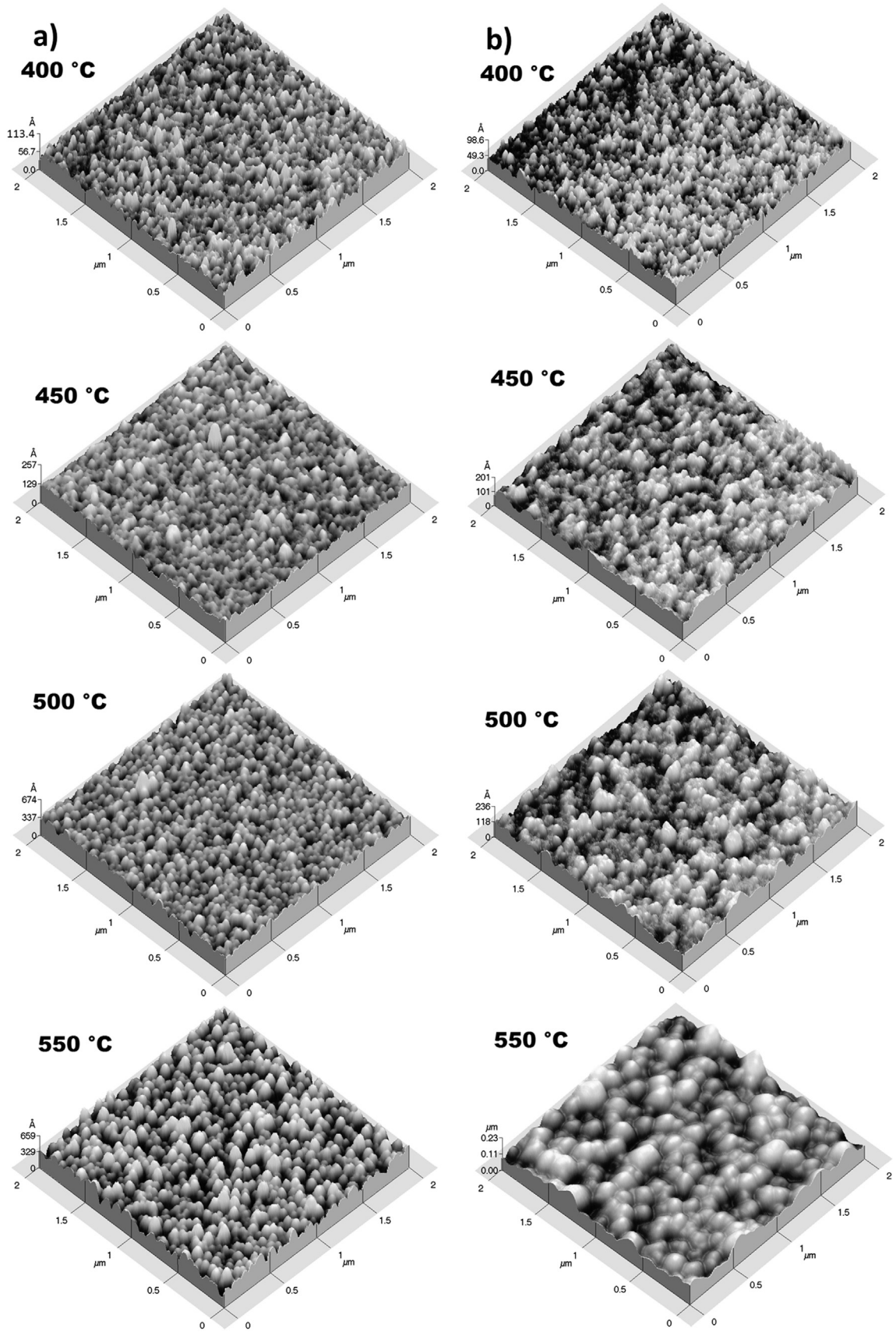

Fig. 3. AFM images for 3a) Y_2O_3:Tb^{3+} and 3b) Y_2O_3:Eu^{3+} thin films deposited at temperatures from 400 to 550 °C.

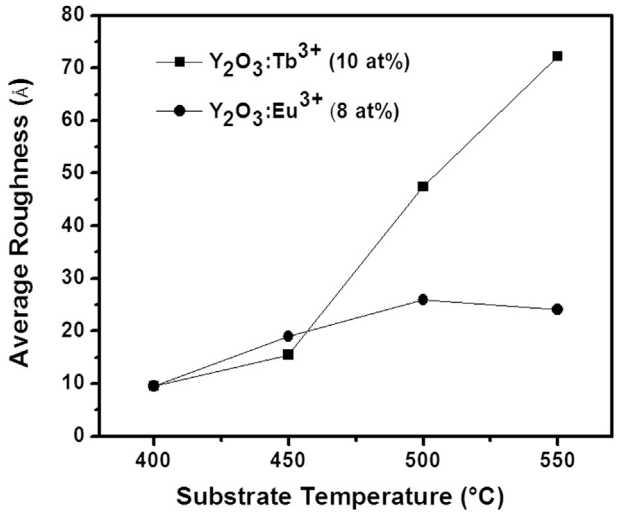

Fig. 4. Average roughness variation of Y_2O_3:Tb^{3+} and Y_2O_3:Eu^{3+} thin films as a function of substrate temperature.

Y_2O_3:Tb^{3+} films and 9.54 to 25.9 Å for Y_2O_3:Eu^{3+} films as illustrated in Fig. 4 where the average roughness of Y_2O_3:Tb^{3+} and Y_2O_3:Eu^{3+} thin films as a function of substrate temperature are presented. This increase in roughness could be due to the formation of the crystalline phase as well as incremented grain size, as seen in the XRD diffractograms (Fig. 1).

UV–vis % transmittance measurements (Fig. 5) were performed on samples deposited on fused quartz slides in order to determine the transparency for Y_2O_3:Tb^{3+} and Y_2O_3:Eu^{3+} films. In this case the curves correspond to a thin films deposited at 550 °C and doped with 8 at% of Eu^{3+} ions (a), and 10 at% of Tb^{3+} ions (b). The % transmission value is greater than 90% in both cases, for wavelengths in the UV–vis region above 250 nm. Also, the transmission of Y_2O_3:Tb^{3+} thin films is similar to the transmission of Y_2O_3:Eu^{3+} thin films. This characteristic is useful for applications in electroluminescent devices [23]. The refractive index values of the films showed a value close to 1.81, indicating relatively dense films.

EDS measurements for the films studied are listed in Tables 1 and 2. The incorporation of Eu in the films is less efficient (Table 1) and more sensible to deposition temperature (Table 2) than the one observed for Tb.

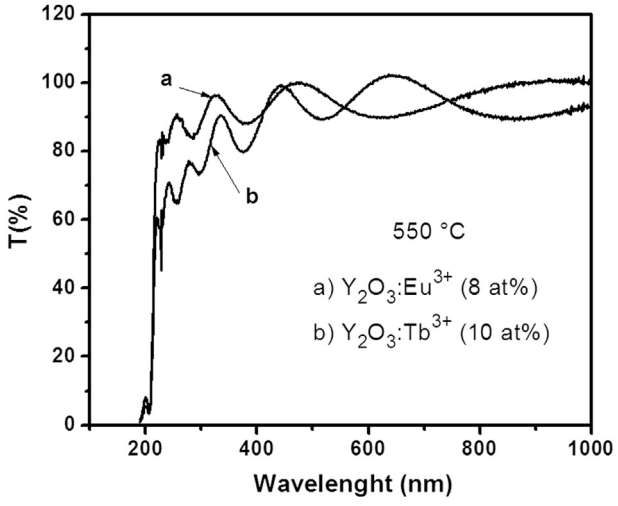

Fig. 5. Typical transmission spectra in the UV–vis region for a) Y_2O_3:Tb^{3+} and b) Y_2O_3:Eu^{3+} thin films synthesized at 550 °C.

Table 1
Atomic percent content of the oxygen, yttrium and europium/terbium, as determined by EDS in films deposited at 550 °C, for different $EuCl_3$/$TbCl_3$ concentration into the spraying solution.

Dopant concentration in spraying solution	Eu doped films (at. %)			Dopant concentration in spraying solution	Tb doped films (at. %)		
	O	Y	Eu		O	Y	Tb
0	63.00	37.00	0	**0**	60.45	39.55	0.0
2	62.15	37.60	0.25	**2**	63.36	36.21	0.43
5	61.35	38.18	0.47	**5**	62.39	36.63	0.98
8	60.14	38.73	1.13	**10**	62.15	35.72	2.13
10	60.12	38.31	1.57	**15**	60.18	36.89	2.93
12	59.30	38.48	2.22				

Fig. 6 shows the excitation spectra for both, Tb^{3+} and Eu^{3+} doped films. Y_2O_3:Tb^{3+} films (Fig. 6a) show a broad excitation peak for the 547 nm luminescent emission peak, in the wavelength range from 245 to 340 nm, centered at 308 nm. This band is attributed to a charge transfer from, either the metal-ligand (Tb^{3+}–O^{2-}) of the oxygen 2*p* orbital to the terbium 4*f* orbital, or due to an ($4f^8$ to $4f^7 5d^1$) interconfigurational transition [24–26]. The excitation spectrum for Y_2O_3:Eu^{3+}, (Fig. 6b) shows a symmetrical relatively narrow band in the wavelength range from 225 to 280 nm with maximum intensity for 256 nm. This band is due to the charge transfer from the metal-ligand (Eu^{3+}–O^{2-}), where an electron jumps from oxygen to europium and is given by $4f^6$ to $4f^7$ O^{-1} transition. This narrow peak is in contrast to the broad excitation band of the Y_2O_3:Tb^{3+} thin films, which is quite probably due to the short inter-nuclear distance between Eu^{3+} activator ion and O^{2-} ligand in configurational coordinate [25]. Excitation peaks associated with inter electronic energy levels of Eu^{3+} ion shown in the inset of Fig. 6b are narrow and small. These peaks are observed at 324, 365, 384 and 395 nm excitation wavelengths assigned to $^7F_0$ to $^5D_4$, $^7F_0$ to $^5G_3$, $^7F_0$ to $^5L_6$ transitions respectively [27].

Fig. 7 shows PL emission intensity behavior for both Y_2O_3:Tb^{3+} and Y_2O_3:Eu^{3+} thin films as a function of wavelength for different doping concentrations in the precursor solution. In the spectra for Y_2O_3:Tb^{3+} films (Fig. 7a), four bands are distinguished which are associated to $^5D_4$ to ^7F_J ($J = 6, 5, 4, 3$) electronic energy level transitions. Also is observed that the most intense radiation emission band is located at 547 nm ($^5D_4$ to $^7F_5$) showing a dominant green light emission. The inset in this figure shows that the highest emission intensity was obtained for 10 at% of Tb^{+3} in precursor solution, while for concentrations higher than 10 at% a concentration quenching was observed. In the photoluminescence emission spectra for Y_2O_3:Eu^{3+} thin films (Fig. 7b), four bands are observed which are assigned to $^5D_1$ to $^7F_1$ and $^5D_0$ to ^7F_J ($J = 1, 2, 3$) electronic energy level transitions. Also, the most intense emission band is located at 611 nm ($^5D_0$ to $^7F_2$) showing a dominant red light emission. The highest emission intensity, in this case, was obtained for 8 at% of Eu^{+3} in the spraying solution; doping concentrations higher than 8 at% causes a concentration quenching (inset of Fig. 7b).

Table 2
Atomic percent content of the oxygen, yttrium and europium/terbium as determined by EDS in films doped with 8/10 at% content of $EuCl_3$/$TbCl_3$, for different substrate temperatures.

Substrate temperature (°C)	Eu doped films (at. %)			Tb doped films (at. %)		
	O	Y	Eu	O	Y	Tb
400	62.59	35.03	2.38	58.23	39.39	2.38
450	62.15	35.90	1.95	57.41	40.43	2.16
500	61.23	37.10	1.67	58.93	39.05	Tb
550	60.14	38.73	1.13	59.13	38.93	2.38

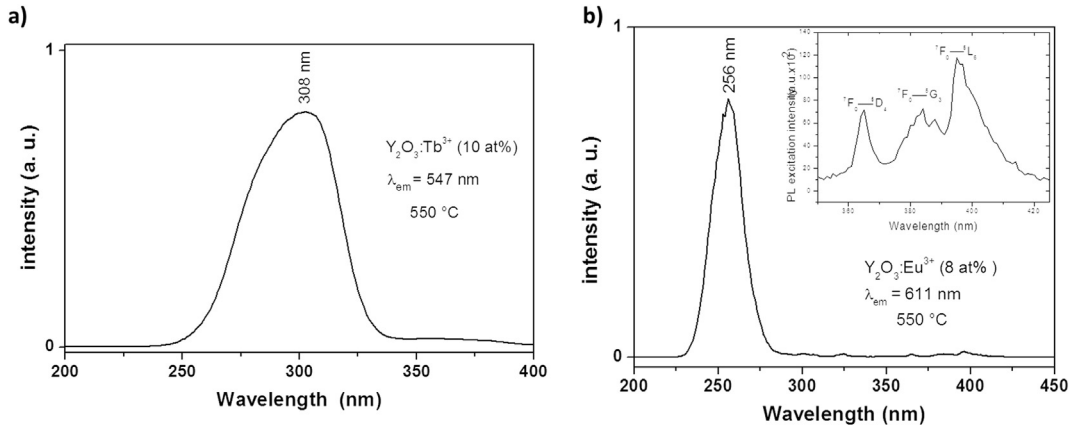

Fig. 6. Excitation spectra obtained for 6a) $Y_2O_3:Tb^{3+}$ and 6b) $Y_2O_3:Eu^{3+}$ thin films synthesized at 550 °C. Emission wavelengths for Tb^{3+} and Eu^{3+} were fixed at 547 and 611 nm, respectively.

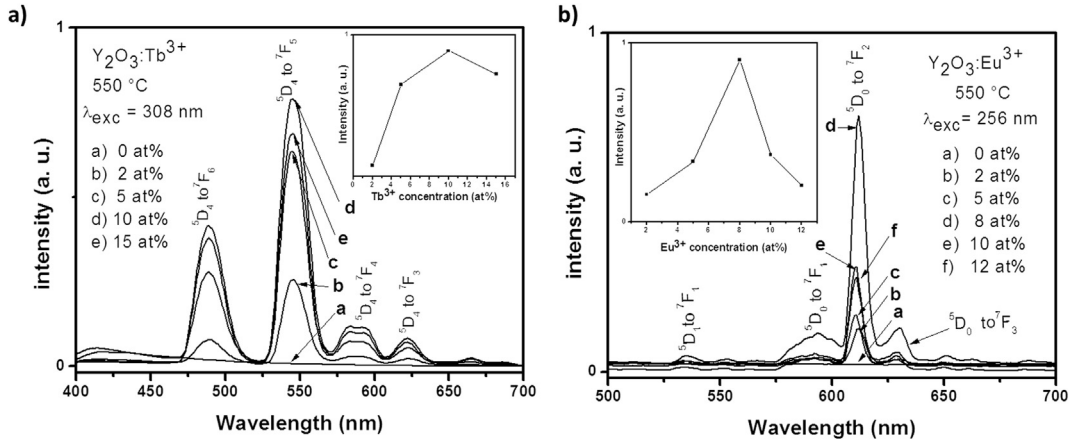

Fig. 7. PL emission intensity spectra for 7a) $Y_2O_3:Tb^{3+}$ and 7b) $Y_2O_3:Eu^{3+}$ thin films with variations in the doping concentration, deposited at 550 °C, under excitation at 308 and 256 nm respectively.

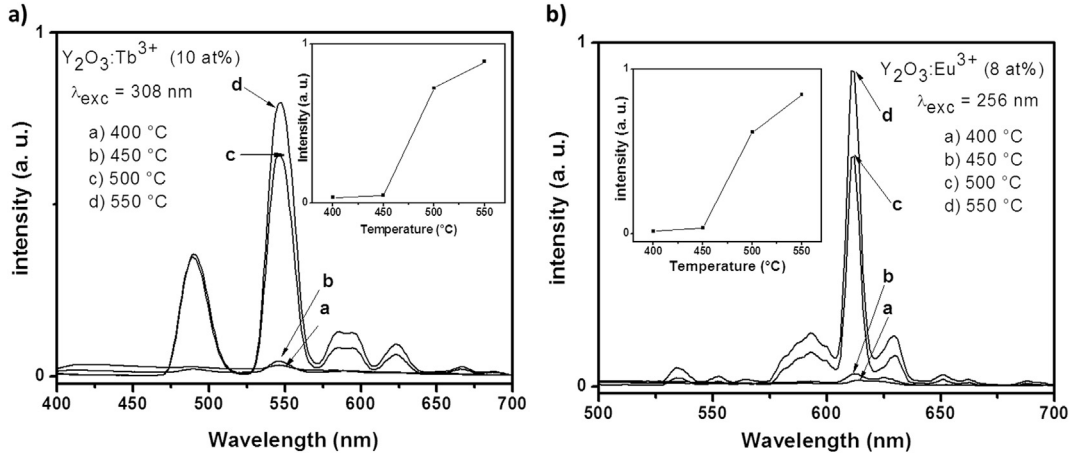

Fig. 8. PL emission intensity spectra as a function of different substrate temperatures for 8a) $Y_2O_3:Tb^{3+}$ and 8b) $Y_2O_3:Eu^{3+}$ thin films excited with wavelengths of 308 and 256 nm respectively.

Fig. 8 shows the PL emission intensity for $Y_2O_3:Tb^{3+}$ and $Y_2O_3:Eu^{3+}$ thin films deposited at substrate temperatures from 400 to 550 °C, using an excitation wavelength of 308 and 256 nm, respectively. It is observed that for 400 and 450 °C, a quite weak PL is present. However, the PL emission intensity is increased in the films deposited at 500 °C, and the maximum emission intensity corresponds to the films synthesized at 550 °C (shown in the inset of Fig. 8a and b). The maximum deposition temperature was 550 °C

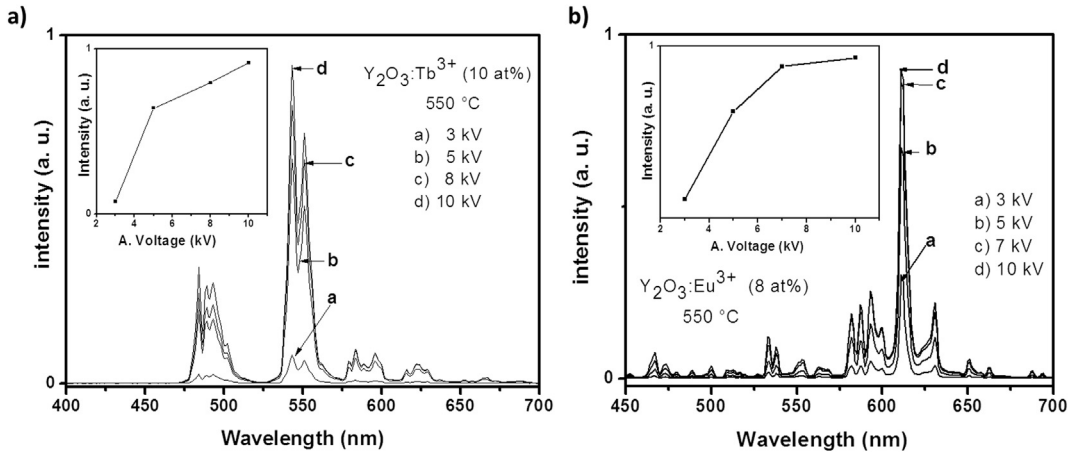

Fig. 9. CL emission intensity spectra for 9a) $Y_2O_3:Tb^{3+}$ and 9b) $Y_2O_3:Eu^{3+}$ thin films, varying electron acceleration voltage. These films were deposited at substrate temperature of 550 °C.

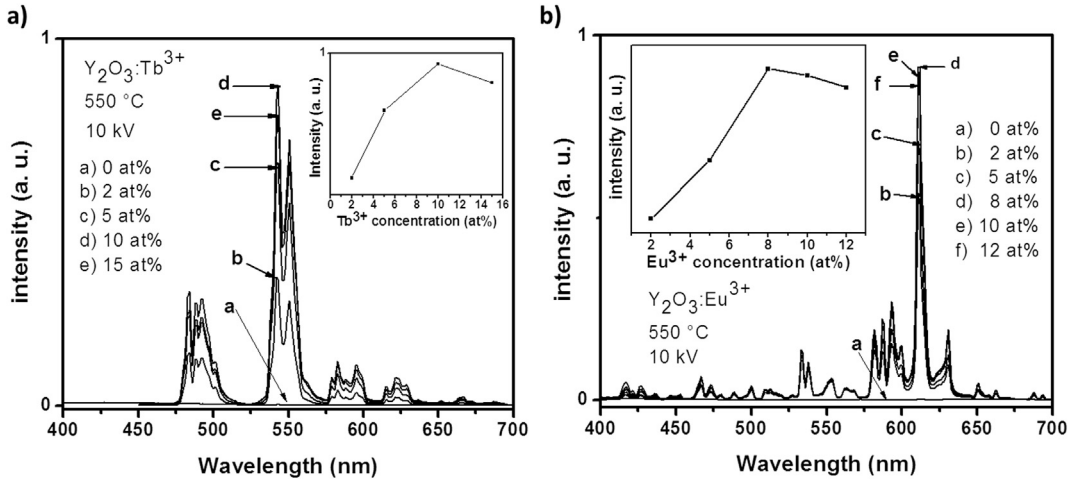

Fig. 10. CL emission intensity spectra for 10a) $Y_2O_3:Tb^{3+}$ and 10b) $Y_2O_3:Eu^{3+}$ thin films as a function of doping concentration. The substrate temperature was 550 °C and electron acceleration voltage was 10 kV.

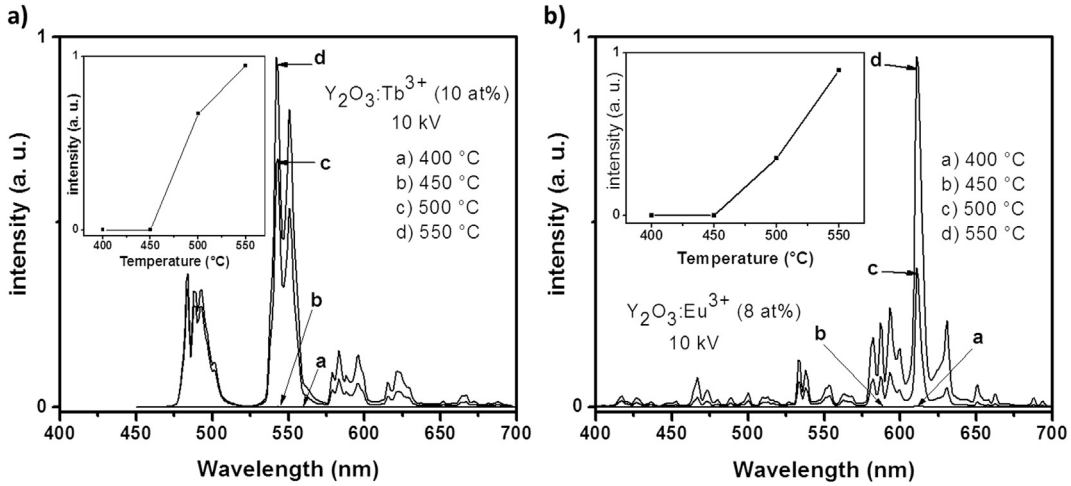

Fig. 11. CL emission intensity spectra for 11a) $Y_2O_3:Tb^{3+}$ and 11b) $Y_2O_3:Eu^{3+}$ thin films as a function of the substrate temperature. The electron acceleration voltage was 10 kV.

due to technical limitations in our synthesis method. It is likely that the improved crystallinity obtained with high deposition temperatures caused that Tb^{3+} and Eu^{3+} ions had a better location within the host crystallites and consequently, the emission intensity was increased.

Cathodoluminescence (CL) measurements were performed in Y_2O_3:Tb^{3+} and Y_2O_3:Eu^{3+} films deposited with 10 at% of Tb^{3+} and 8 at% of Eu^{3+} and substrate temperature of 550 °C using an electron acceleration voltage in the 3–10 kV range (Fig. 9), in order to find the optimum voltage for maxima emission; although in practical applications lower acceleration voltages are used. In these spectra it is distinguished that the highest intensity corresponded to the emission spectrum with an acceleration voltage at 10 kV. Because of the increased acceleration voltage, the penetration of the electrons in the material is higher. They produced more electron–hole pairs. These pairs excite more activator centers due to their interaction with a larger volume of the luminescent material; therefore CL emission intensity is incremented. In addition, it was observed that the emission bands had a distortion, probably due to the acceleration voltage.

The acceleration voltage at 10 kV was also used in films deposited with different doping concentration and different substrate temperatures. Fig. 10 shows CL emission intensity spectra for Y_2O_3:Tb^{3+} and Y_2O_3:Eu^{3+} films as a function of wavelength for doping concentration in the range from 0 to 15 at% for Y_2O_3:Tb^{3+} thin films and in the range from 0 to 12 at% for Y_2O_3:Eu^{3+} thin films. These films were deposited at 550 °C. Behavior of the CL emission bands is similar to the PL emission bands; the insets in both Figs. 7 and 10 show these results. Also it was observed that since the four bands $^5D_4$ to ^7F_J ($J = 6, 5, 4, 3$) for Tb^{3+} and $^5D_1$ to $^7F_1$, $^5D_0$ to ^7F_J ($J = 1, 2, 3$) for Eu^{3+} have high J values, the crystal field splits the levels in several sublevels which give the spectra a complicated appearance [25]. In Addition, when the doping concentration is incremented at 15 at% of Tb^{3+} and 10 at% of Eu^{3+} in the spraying solution, quenching concentration is observed (inset of Fig. 7a and b, CL emission intensity).

CL emission intensity spectra for Y_2O_3:Tb^{3+} and Y_2O_3:Eu^{3+} thin films as a function of wavelength varying the substrate temperature are shown in Fig. 11. Here, it is observed that as a result of the increase of substrate temperature, the CL emission intensity was also incremented. So the explanation for these results is very similar to the mentioned for the photoluminescence results. These results confirm that at temperatures of 400 and 450 °C there is a very weak emission.

XRD results shown in Fig. 1 might help to explain the lack of emission at low temperatures (400 and 450 °C). It is observed in these diffractograms that at these temperatures the Y_2O_3:Tb^{3+} and Y_2O_3:Eu^{3+} films were amorphous. Another possible explanation for the weak or absent luminescence in films deposited at 400 and 450 °C can be given by infrared spectroscopy results presented in Fig. 2. The IR spectra for Y_2O_3:Tb^{3+} and Y_2O_3:Eu^{3+} thin films synthesized in the 400–550 °C range show two overlapped bands which are located approximately at 1405 and 1525 cm^{-1}; assigned to δ (CH_3) and ν (C=O) coupled with ν (C=C) vibrations, respectively [16,17]. The band appeared at 872 cm^{-1} can be assigned to π (CH). These three bands are characteristic of the terbium, europium and yttrium β diketonates indicating an incomplete decomposition of the precursors especially at low temperatures. Therefore, these organic functional groups present into the films might be responsible for the degraded photo and cathodoluminescence emissions. In addition at higher temperatures the organic residues are reduced and the Y–O bonds are increased in the Y_2O_3:Tb^{3+} and Y_2O_3:Eu^{3+} thin films deposited at these temperatures (500 and 550 °C) in agreement with the improvement of the crystalline structure of the films as shown in the X-ray results.

4. Conclusions

The synthesis route for yttrium, terbium and europium β diketonates from organic salts and acetylacetone was reported as well as the deposition of Y_2O_3:Tb^{3+} and Y_2O_3:Eu^{3+} films using these compounds as precursors, by the spray pyrolysis technique, at different substrate temperatures and at different doping concentrations. The deposition temperature and the crystalline structure of these films influenced strongly the PL and CL emission intensities. Films synthesized at high substrate temperatures have a strong luminescent intensity. Spectra of Y_2O_3:Tb^{3+} thin films have a dominant peak located at 547 nm, a green light emission, due to $^5D_4$ to $^7F_5$ electronic transitions associated with Tb^{3+} ions. In the case of Y_2O_3:Eu^3 films, the main peak is located at 611 nm, a red light emission, due to $^5D_0$ to $^7F_2$ electronic transitions associated with Eu^{3+} ions. Best experimental conditions to obtain maximum emission intensity for Y_2O_3:Tb^{3+} films were: doping concentration about 10 at% of Tb^{3+} (inside the precursor solution) and substrate temperature at 550 °C; also a concentration quenching was observed for doping concentrations greater than 10 at%. In the case of Y_2O_3:Eu^{3+} the optimum doping concentration was about 8 at% of Eu^{3+} in films deposited at 550 °C; also, a quenching effect was observed for doping concentration greater than 8 at%.

At high temperatures, the crystalline phase of Y_2O_3 was improved. Thin films deposited at higher substrate temperatures showed a low average surface roughness of 62 Å for Y_2O_3:Tb^{3+} and 25 Å for Y_2O_3:Eu^{3+} thin films. The films presented in this work were dense, and showed a 1.81 index of refraction, as well as a high optical transmittance in the UV–vis range of the electromagnetic spectrum, suggesting the possibility to be applied in electroluminescent devices.

Acknowledgments

The authors would like to thank SECITI (before ICyTDF) project # PICSO 12-119, to DGAPA-UNAM, SIP-IPN and CONACyT for the financial support through the scientific research projects (Grant Nos. 129227, 20130236, 20130153, 20140458 and 20140459). The technical assistance of M. Guerrero, Z. Rivera, A. B. Soto and J. Carmen Flores is also acknowledged.

References

[1] Albert G. Nasibulin, Esko I. Kauppinen, David P. Brown, Jorma K. Jokiniemi, J. Phys. Chem. B 105 (2001) 11067.
[2] M. Aguilar-Frutis, G. Reyna-García, M. García-Hipólito, J. Guzmán-Mendoza, C. Falcony, J. Vac. Sci. Technol. A22 (4) (2004) 1.
[3] G. Alarcón-Flores, M. Aguilar-Frutis, C. Falcony, M. García-Hipólito, J.J. Araiza-Ibarra, H.J. Herrera-Suárez, J. Vac. Sci. Technol. B 24 (4) (2006) 1873.
[4] G. Alarcón-Flores, M. Aguilar-Frutis, M. García-Hipólito, J. Guzmán-Mendoza, M.A. Canseco, C. Falcony, J. Mater. Sci. 43 (2008) 3582–3588.
[5] Jun Yeol Cho, Ki Young Ko, Young Rag Do, Thin Solid Films 515 (2007) 3373–3374.
[6] C. Falcony, A. Ortiz, J.M. Dominguez, M.H. Farias, L. Cota Araiza, G. Soto, J. Electrochem. Soc. 139 (1) (1992) 267.
[7] J. Aarik, H. Mändar, M. Kira, L. Pung, Thin Solid Films 466 (2004) 41–47.
[8] V. Swamy, N.A. Dubrovinskaya, L.S. Dubrovinskaya, J. Mater. Res. 14 (2) (1999) 456.
[9] J. Mouzon, Licenciate Thesis, Lulea University of Technology, 2005.
[10] R.N. Bhargava, J. Luminescence 70 (1996) 85.
[11] E.T. Goldburt, B. Kulkarni, R.N. Bhargava, J. Taylor, M. Libera, J. Luminescence 72-74 (1997) 190–192.
[12] R.K. Singh, Z. Chen, D. Kumar, K. Cho, M. Ollinger, Appl. Surf. Sci. 197-198 (2002) 321.
[13] R.C. Mehrotra, R. Bohra, D.P. Gaur, Metal β Diketonates and Allied Derivatives, Academic Press, London LTD, 1978, p. 268.
[14] W. Sheng-Yue, Lu Zu-Hong, Mater. Chem. Phys. 78 (2002) 542.
[15] B.D. Cullity, in: Morris Cohen (Ed.), Elements of X-ray Diffraction, Addison-Wesley Publishing Company Inc., Reading M.A., 1956, p. 99.
[16] O. Stryckmans, T. Segato, P.H. Duvigneuud, Thin Solid Films 283 (1996) 19.

[17] K. Nakamoto, Infrared and Raman Spectra of Inorganic and Coordination Compounds 4, John Wiley and Sons, USA, 1986, pp. 259–268.
[18] M. Aguilar-Frutis, M. Garcia, C. Falcony, Appl. Phys. Lett. 72 (14) (1998) 1700.
[19] M. Aguilar-Frutis, M. Garcia, C. Falcony, G. Plesch, S. Jimenez, Thin Solid Films 389 (2001) 200.
[20] H. Guo, W. Zhang, L. Lou, A. Brioude, J. Mugnier, Thin Solid Films 458 (2004) 276.
[21] S.A. Barve, Jagannath, N. Mithal, M.N. Deo, A. Bisajas, R. Mishra, R. Kishore, B.M. Bhanage, L.M. Gantayet, D.S. Pati, Thin Solid Films 519 (2011) 3016.
[22] Y. Repelin, C. Proust, E. Husson, J.M. Beny, J. Solid State Chem. 118 (1995) 163–169.
[23] Y.A. Ono, Electroluminescence, in: Encyclopedia of Applied Physics, vol. 5, VCH Publishers Inc, 1993.
[24] J.Y. Choe, D. Ravichandran, S.M. Blomquist, K.W. Kirchner, E.W. Forsythe, D.C. Morton, J. Luminescence 93 (2001) 119–128.
[25] G. Blasse, B. Grabmaier, Luminescent Materials, Springer-Verlag, 1994.
[26] B. Lei, Y. Liu, G. Tang, Z. Ye, C. Shi, Mater. Chem. Phys. 87 (2004) 227–232.
[27] M.K. Chong, K. Pita, C.H. Kam, J. Phys. Chem. Solids 66 (2005) 214.